PROCEEDINGS OF SCIENCE

Energy estimation of atmosphere-skimming cosmic ray events using the radio technique

Sergio Cabana-Freire,[a,*] **Jaime Alvarez-Muñiz**[a] **and Matias Tueros**[b]

[a] *Instituto Galego de Física de Altas Enerxías (IGFAE), Universidade de Santiago de Compostela, 15782 Santiago de Compostela, Spain*

[b] *Instituto de Fisica La Plata, CONICET-UNLP, Diagonal 113 entre 63 y 64 , La Plata, Argentina*

E-mail: sergio.cabana.freire@usc.es, jaime.alvarez@usc.es, tueros@fisica.unlp.edu.ar

Cosmic rays can induce extensive air showers whose development takes place entirely inside the atmosphere, without reaching the ground. These atmosphere-skimming events have been detected with balloon-borne experiments such as ANITA and EUSO-SPB2. In this work, we evaluate the possibility of estimating the energy of an atmosphere-skimming cosmic ray shower through measurements of radio pulses. We report on the performance of an energy reconstruction method which adapts existing algorithms to the peculiar characteristics of atmosphere-skimming events, and study its accuracy for different event geometries, and in different scenarios of angular resolution and signal-to-noise ratio.

39th International Cosmic Ray Conference (ICRC2025)
15 - 24 July 2025
Geneva, Switzerland

*Speaker

PoS(ICRC2025)208

1. Introduction.

Ultra-high energy cosmic rays (UHECR) with trajectories that do not intercept the Earth's surface can induce particle cascades that develop entirely inside the atmosphere, without any shower component ever reaching the ground. Several of these *atmosphere-skimming* air shower events have been detected in the past aboard balloon-borne experiments, such as ANITA [1] and EUSO-SPB2 [2] through the radio and Cherenkov emission associated to the air shower, respectively. High-altitude radio-based experiments to be deployed in the near future, such as PUEO [3] and POEMMA - Balloon with Radio (PBR) [4], are expected to increase the number of detected atmosphere-skimming events, thanks to their improved sensitivities.

The properties and typical length scales of atmosphere-skimming air showers can differ significantly from those of downward-going cascades. Since the shower evolves mainly through low density layers of the atmosphere, the longitudinal development of the cascade can span distances of hundreds of kilometers. Meanwhile, the geomagnetic field gives rise to highly asymmetric shower fronts, elongated laterally along the direction of the local Lorentz force [5].

The increased longitudinal and lateral dimensions of these particle cascades have a non trivial impact on the properties of the emitted radio pulses, that need to be studied through detailed simulations [6]. In general, the frequency up to which the particles in the cascade can contribute coherently to the signal is much more limited than in the case of downward-going showers, due to the enhanced time delays induced by the large length scales involved. Moreover, and for similar reasons, the asymmetric shape of the shower front alters the frequency content of the pulses received inside or outside the plane where the shower front spreads. The altitude-dependent refractive index also has an effect on the off-axis angles where the received pulses are maximally coherent. While in downward-going geometries these positions form a symmetric cone-like region around the shower axis (the so-called *Cherenkov cone*), in atmosphere-skimming events this region becomes asymmetric due to the different optical paths above and below the shower axis.

At the time of their detection by ANITA, the absence of detailed simulations made impossible to perform a dedicated analysis of the recorded atmosphere-skimming events [1]. To fill this gap, in this work we present a simulation-based method that uses radio pulses recorded aboard balloon-borne experiments to estimate the primary particle energy in atmosphere-skimming cosmic ray events.

2. Energy estimation methodology

The method we present in this work to estimate the primary cosmic ray energy from a measured radio pulse, produced by an atmospheric-skimming air shower, is based on the procedure applied to the cosmic ray air shower events recorded during the first flight of ANITA [7], where the detected radio pulses underwent a reflection in the ice cap of Antarctica before reaching the detector. In this work we adapt this energy reconstruction method to the geometries of atmosphere-skimming events.

Simulations of radio pulses from these events, revealed amplitude spectra $A(f)$ decreasing exponentially with frequency, with the approximate shape:

$$A(f) = A_0 \, e^{\gamma(f - f_0)} \, . \tag{1}$$

The amplitude of the spectrum A_0 (at a reference frequency f_0) depends on the primary energy, which determines the number of particles contributing to the emission, but also on the off-axis position of the observer as this affects the coherence of the received signal. On the other hand, the spectral slope γ is found to depend strongly on the off-axis angle at which the radio pulse is observed, with a weak dependence on primary energy. By measuring γ and comparing it to that obtained in shower simulations with geometries compatible with the direction of the received pulse, the spectral amplitude at the Cherenkov cone can be inferred. This allows to obtain an observable that correlates directly with the primary energy.

2.1 Selection of compatible shower geometries

The energy reconstruction method is based on comparing the measured electric field spectrum with simulations of air showers, whose geometries need to be compatible with the direction of the received radio pulse. For atmosphere-skimming showers, the only information available is the arrival direction of the radio pulse $(\theta_{\text{pulse}}, \phi_{\text{pulse}})$ at the altitude of the detector (h_D)[1]. The selection of shower geometries is based on the assumption that the incoming direction of the radio pulse *points back* to the depth of shower maximum development, X_{max}, as shown in figure 1. This assumption treats the emission as originating from a point source, consistent with the expectation that most of the radio emission arises from a region near the cascade maximum.

The selection proceeds in two main steps. First, assuming a primary cosmic ray energy E_0, we place $X_{\text{max}}(E_0)$ at different positions and select those compatible with the incoming direction of the radio pulse, and find the appropriate impact parameters b for the corresponding showers as indicated in the two examples in Fig. 1a. The distance between the observer and X_{max}, together with the impact parameter b, are sufficient to determine the orientation of the shower axis relative to the observer.

In the second step, we reject shower geometries for which X_{max} cannot be observed from the position of the detector at an off-axis angle ψ smaller than a specified value. By repeating the process for other primary energies and applying the same selection, a set of compatible shower geometries to be simulated is obtained. Further details about these two steps are provided in the following.

Compatibility between X_{max} at a given energy and pulse incoming direction: Given that the only available experimental information is the arrival direction of the pulse, at each tested energy the simulated atmosphere-skimming showers are chosen so that their X_{max} matches the expected average depth of shower maximum $\langle X_{\text{max}} \rangle$ for showers at that energy. Depending on the objectives of the reconstruction, this $\langle X_{\text{max}} \rangle$ could be taken either from real measurements by other experiments or from the simulation prediction for a given primary type. In this work, we will focus on proton primaries.

Once $\langle X_{\text{max}} \rangle(E_0)$ is fixed and an atmospheric density profile is chosen, it can be shown that for any primary energy and position seen by the detector under an angle θ_{pulse}, there is a unique shower geometry with $\langle X_{\text{max}} \rangle$ at that position. This is sketched in Fig. 1a, where for all possible shower axis passing through the same point, there is only one value of b such that the average depth of X_{max} occurs at that position.

[1] In the case of ANITA, the pulse arrival direction is determined using interferometric techniques [1].

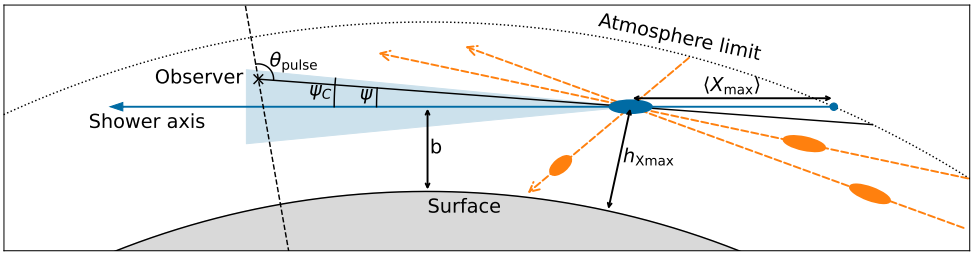

(a) Showers with X_{max} inconsistent with the incoming direction of the radio pulse (dashed orange arrows), and a shower with a compatible X_{max} (solid blue arrow) seen at off-axis angle $\psi \lesssim \psi_C$.

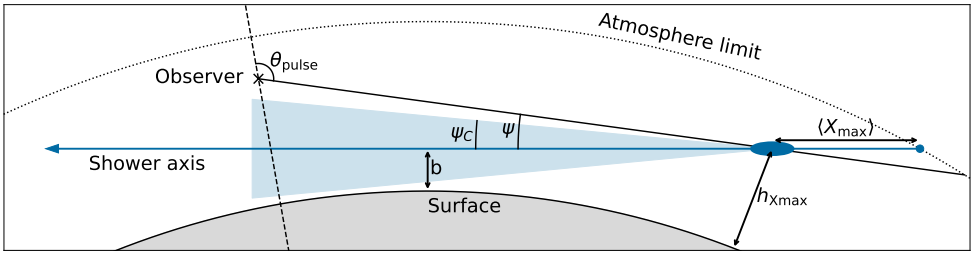

(b) Shower with an X_{max} compatible with the pulse incoming direction, but seen at off-axis angle $\psi > \psi_C$.

Figure 1: Sketch of the shower selection procedure (not to scale). The observer receives a radio pulse with incoming direction defined by the angle θ_{pulse}. See text for details.

Rejection of shower geometries seen at large off-axis angles ψ: The frequency content of the signals produced by an atmosphere-skimming shower drops rapidly when moving away from the Cherenkov angle. This makes it unlikely to detect a radio pulse far from the off-axis angle where coherence is maximal ψ_C. By placing a cut on the off-axis angle at the observer position, we can further constrain shower geometries capable of producing the observed pulse. This is sketched in figure 1, where the $X_{\text{max}}(E_0)$ of both candidate air showers (solid blue arrows) is seen under an angle θ_{pulse}, but only the maximum of shower (a) would be seen at a small enough off-axis angle to potentially trigger a detection.

The off-axis angle where the received signal is maximally coherent ψ_C corresponds to the observer position where time delays between individual emissions in the air shower are minimal. Using a 1D model for the air shower longitudinal development, we calculate numerically the expected time delays at the plane of the detector, accounting for the differences in optical paths. The result of this approach is exemplified in figure 2 for four shower geometries compatible with a pulse received with $\theta_{\text{pulse}} = 94.5°$. The positions where time delays are minimal (blue rings in fig. 2) define the *effective* Cherenkov angle ψ_C, while the minimal off-axis angle at which the pulse could be seen is denoted as ψ_{min}. For example, in the middle-left panel, a detector at $h_D = 36\,\text{km}$ of altitude would observe X_{max} at an off-axis angle ψ always larger than $\psi_{\text{min}} = 0.5\psi_C$, and it is more likely to be observed than in the right-most panel, where the shower maximum cannot be seen from the same altitude at an off-axis angle smaller than $\psi_{\text{min}} \simeq 2\psi_C$. In fig. 2, rejecting for example all geometries whose X_{max} cannot be seen from an off-axis angle smaller than ψ_C, would constrain the distance between shower maximum and detector to the interval between 766 and 788 km.

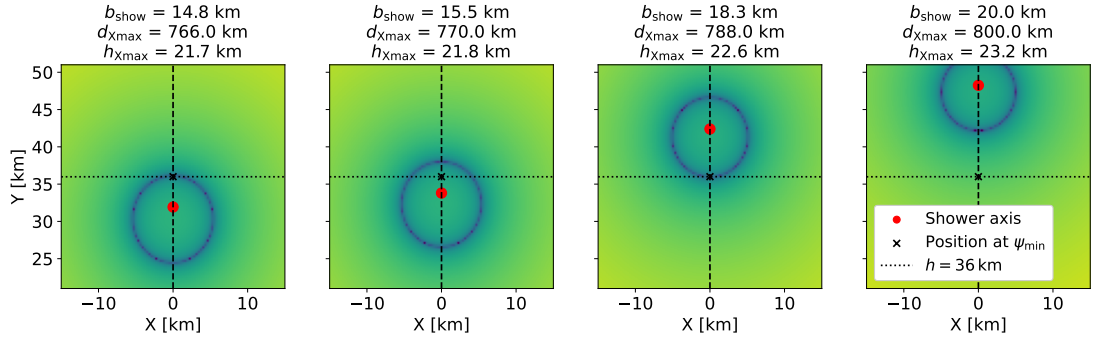

Figure 2: Expected shape of the *Cherenkov ring* in a plane containing a detector hovering at $h_D = 36$ km a.s.l., for different shower geometries compatible with a pulse direction of $\theta_{\text{pulse}} = 94.5°$. The dashed vertical line represents the vertical of the observer, as in fig. 1. The regions in blue correspond to the positions where time delays from a 1D shower would be minimal. The shower axis *enters* the figure *through* the red dot. The smaller off-axis angle at which the pulse can be seen is denoted as ψ_{min}. The impact parameter b of each shower axis, as well as the height of X_{max} and its distance to the detector d_{Xmax}, are indicated above each panel.

2.2 Exponential modeling of the electric field spectrum

The energy reconstruction method relies on fitting the amplitude spectrum $A(f)$ of the received electric field to the exponential function in equation (1) in the frequency range $200 - 450$ MHz, choosing $f_0 = 300$ MHz. This is different to the frequency range adopted in the analysis of reflected radio pulses in ANITA I ($300 - 1000$ MHz). This change is motivated by the reduction of the high frequency content of radio pulses expected in atmosphere-skimming air showers [6]. Low-frequency instruments working in the $50 - 500$ MHz are to be included in the PUEO [8] and PBR [4] payloads, and are expected to increase the sensitivity to atmosphere-skimming air showers [8].

An example of a simulated radio pulse produced in an atmosphere-skimming air shower is presented in figure 3, after applying a rectangular filter in the $50 - 500$ MHz frequency range and adding random gaussian noise. In the right panel, a clear exponential shape is seen for the spectrum of the simulated signal. Despite the presence of noise, estimators for the signal amplitude can be obtained using Rician statistics, following methods similar to those employed in [7, 9]. In the example shown, a ~ 250 ns long time trace sampled at 10 GSa/s is enough to estimate the signal spectrum.

In Fig. 4 we show the results of the exponential fits at different off-axis angles, obtained from simulated atmosphere-skimming showers of different energies and with geometries compatible with the arrival direction of the pulse shown in Fig. 3. The spectral amplitude A_0 at $f_0 = 300$ MHz (left panel) depends on the off-axis angle, peaking at $\psi = \psi_C \sim 0.36°$, corresponding to the effective Cherenkov angle, and increases with primary energy, as expected. The spectral slope γ (central panel) is also maximal around the same off-axis angle, since signals around the Cherenkov angle have higher frequency content and thus flatter spectra. There is not a clear dependence of γ with the primary energy and, as a consequence, the simulated spectral parameters are clustered along lines in the $\gamma - \log_{10} A$ plane, with an offset that increases linearly with the logarithm of simulated primary energy (right panel in fig. 4). For a measured event, estimating the *offset* with respect to a calibration line in this plane, allows to obtain an estimate of the primary particle energy.

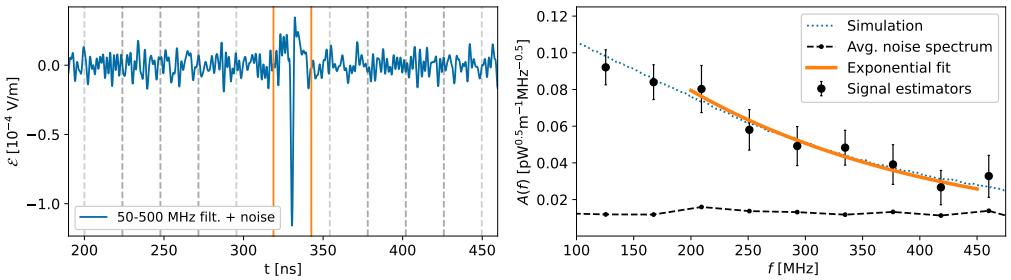

Figure 3: Simulated radio pulse produced by an atmosphere-skimming proton-induced air shower, of energy $E = 10^{18}$ eV. Left: Time domain electric field after filtering in the $50-500$ MHz frequency range and adding random gaussian noise. Right: Amplitude spectrum of the pulse in the left panel in the frequency domain. The pulse is observed at an altitude of 36 km a.s.l. with an incoming angle $\theta_{\rm pulse} \sim 94.66°$. The average noise spectrum is estimated from several *noise windows* (dashed vertical lines in the left panel) around the *signal* window (solid vertical lines).

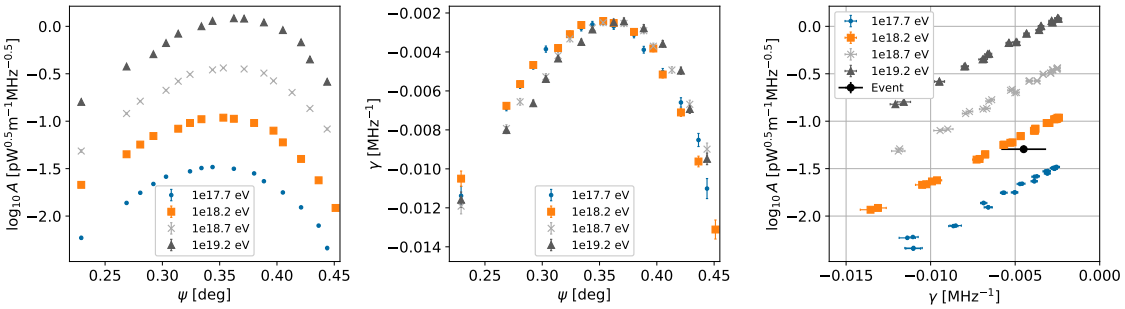

Figure 4: Results of fitting the amplitude spectrum to the exponential function in equation (1) for atmosphere-skimming air showers with varying energies and geometries, compatible with that of the example event shown in fig. 3. The spectral parameters A_0 and γ are displayed in the left and center panels as a function of off-axis angle, and plotted against each other in the right panel. See text for further details.

3. Validation of the energy estimation method

The performance of the energy estimation method described above was evaluated with a set of 22 reference simulated radio pulses obtained in proton-induced air showers of energy 10^{18} eV, detected at an altitude $h_D = 36$ km a.s.l. with different incoming angles ($\theta_{\rm pulse}$ in fig. 1), and at various off-axis angles. For each of these pulses, firstly we found compatible shower geometries by choosing events with the average $X_{\rm max}$ of proton showers, as predicted with the SIBYLL 2.3d hadronic model [10]. The simulations used for the reconstruction of the energy of the 22 reference showers, were done for primary energies of $\log_{10}(E/{\rm eV}) = 17.7-18.2-18.7-19.2$. Five compatible shower geometries were chosen for each energy, requiring at least one observer at an off-axis angle $\psi < 1.5\,\psi_C$ (see fig. 2). Both the reference and calibration simulations were performed with the ZHAIRES-RASPASS code [11], using the same geomagnetic field and atmospheric model in all cases. In this way, the differences between the true and reconstructed energy would in principle arise from the selection of compatible shower geometries, and event-to-event fluctuations. In a detailed reconstruction of measured events, it would however be necessary to include a realistic

atmospheric model and magnetic field at the position of $X_{\max}$, either obtained from measurements or through reference models, so as to account for the effect of the asymmetric shower fronts in the properties of the radio pulses [5, 6]. This can be easily implemented in the proposed energy reconstruction method, since the position of $X_{\max}$ in the showers used for calibration is fixed by the geometrical selection described in section 2.1.

Random gaussian noise was added to the reference pulses before finding the spectral parameters (A, γ), as exemplified in figure 3. After this, the primary energy is estimated as an average of the reconstructed energies for each one of the compatible geometries. To account for the effect of ambient random noise on the reconstructed energy, we repeated the process multiple times for each event to estimate the average reconstructed energy and its fluctuations. In the following, we define the Signal-to-Noise Ratio as SNR $= \frac{|\max(\mathcal{E})-\min(\mathcal{E})|}{2\sqrt{\langle \mathcal{N}^2 \rangle}}$, with $\mathcal{E}$ and $\mathcal{N}$ the simulated electric field and the noise, respectively.

The average reconstructed energy for this set of events is shown in figure 5, as a function of the incoming angle of the radio pulse, θ_{pulse}.

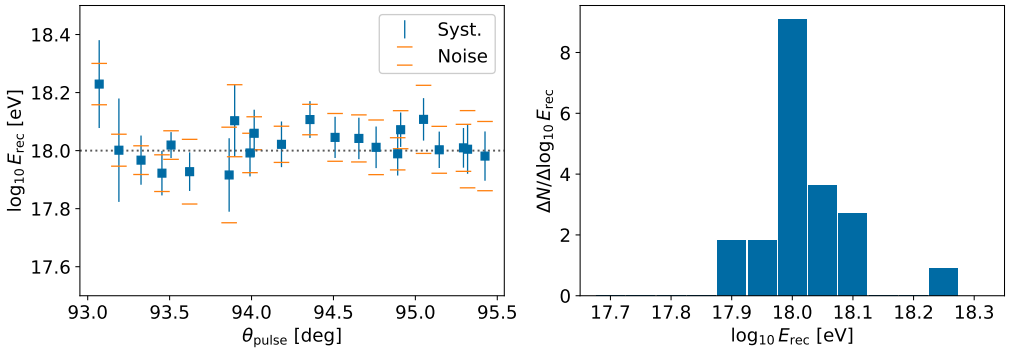

Figure 5: Left panel: Reconstructed $\log_{10}(E_{\text{rec}}/\,\text{eV})$ for the 22 simulated atmosphere-skimming events with true energy $E = 10^{18}$ eV as a function of the incoming direction of the radio pulse (θ_{pulse} in fig. 1), with uncertainties due to differences in the geometry of the calibration showers and noise fluctuations. Right panel: Distribution of reconstructed $\log_{10}(E_{\text{rec}}/\,\text{eV})$. The average SNR is ~ 12.8.

The energy reconstruction method described above recovers, on average, the true value of $\log_{10}(E_{\text{rec}}/\,\text{eV}) = 18$. The width of the distribution of $\log_{10} E_{\text{rec}}$ around this value, of order $\sigma\left(\log_{10} E_{\text{rec}}/\text{eV}\right) \sim 0.07$, corresponds to a typical uncertainty in the primary energy of $\pm\,20\%$ for a SNR $\sim$ 10. Also, there is not an evident bias in the reconstructed energy as a function of the incoming direction of the radio pulse. However, larger event samples would be necessary to address such possibility.

The performance of the energy estimation was further evaluated by applying it to a single event, received with an incoming angle $\theta_{\text{pulse}} \approx 95.15°$, assuming different noise levels, and an uncertainty of the reconstructed incoming direction of the radio pulse up to $\pm\,0.2°$. This value corresponds to the typical angular resolution of ANITA [1]. The results for the energy reconstruction in such scenarios are shown in figure 6. Despite the reduction in SNR, and the introduction of artificial biases in the reconstructed pulse direction, the average value of $\log_{10} E_{\text{rec}}$ is self-consistent in all cases.

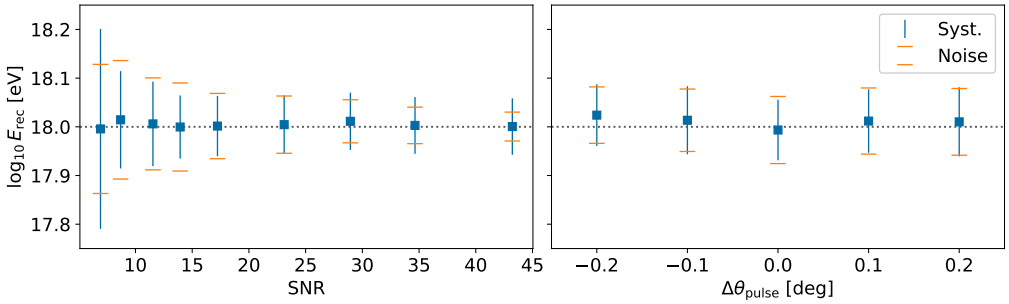

Figure 6: Reconstructed $\log_{10}(E_{\mathrm{rec}}/\,\mathrm{eV})$ for an event seen with elevation angle $\theta_{\mathrm{pulse}} \approx 95.15°$. Left: Results as a function of SNR assuming a perfect reconstruction of the angle θ_{pulse}. Right: Results as a function of the difference $\Delta\theta_{\mathrm{pulse}}$ between the reconstructed and true incoming angle of the radio pulse for a SNR $\sim$ 17.3.

4. Conclusions

The peculiarities of atmosphere-skimming particle cascades, and the effects of the shower geometry and the geomagnetic field in the observed radio emission, need to be studied through realistic and detailed simulations. In this work, we have adapted a previously existing method for reconstructing the primary particle energy, using radio pulses observed from a balloon-borne detector, to the case of atmosphere-skimming geometries. The performance of this method has been evaluated for events with different incoming directions, considering various SNR levels and arrival direction uncertainties. The results presented in this work show a good agreement ($\sim$ 20%) between the true and reconstructed energy for a small sample of events. This methodology sets the basis for the energy reconstruction of atmospheric-skimming events previously recorded by ANITA as well as future experiments such as PUEO and POEMMA - Balloon with Radio. Improvements to the current methodology include optimizing the selection of the simulated air showers needed to calibrate the energy of an event, and optimizing the frequency range where the analysis is performed.

Acknowledgments: Ministerio de Ciencia, Innovación y Universidades/Agencia Estatal de Investigación, MICIU/AEI /10.13039/501100011033, Spain (PID2022-140510NB-I00, PCI2023-145952-2, RYC2019-027017-I, CNS2024-154676, and María de Maeztu grant CEX2023-001318-M); Xunta de Galicia, Spain (CIGUS Network of Research Centers & Consolidación 2021 GRC GI-2033 ED431C-2021/22 and 2022 ED431F-2022/15); Feder Funds.

References

[1] **ANITA** Collaboration, P. W. Gorham *et al.* *Phys. Rev. Lett.* **126** (Feb, 2021) 071103.
[2] **JEM-EUSO** Collaboration, A. Cummings *PoS* **ICRC2023** (2023) 527.
[3] **PUEO** Collaboration, Q. Abarr *et al.* *JINST* **16** no. 08, (2021) P08035.
[4] M. Battisti *et al.* *Nuclear Inst. and Methods in Physics Research A* **1069** (2024) 169819.
[5] M. Tueros *et al.* *JCAP* **2024** no. 07, (Jul, 2024) 065.
[6] M. Tueros *et al.* *JCAP* **2025** no. 01, (Jan, 2025) 112.
[7] H. Schoorlemmer *et al.* *Astropart. Phys.* **77** (2016) 32–43.
[8] **PUEO** Collaboration, Y. Ku *et al.* *PoS* **ARENA2024** (2024) 019.
[9] S. Martinelli *et al.* *Astropart. Phys.* **168** (2025) 103091.
[10] F. Riehn *et al.* *Phys. Rev. D* **102** (Sep, 2020) 063002.
[11] M. Tueros *Zenodo* (2022) .